

Difference-frequency-based tunable absorption spectrometer for detection of atmospheric formaldehyde

David G. Lancaster, Alan Fried, Bryan Wert, Bruce Henry, and Frank K. Tittel

High-sensitivity detection of formaldehyde (CH_2O) at $3.5315\ \mu\text{m}$ ($2831.64\ \text{cm}^{-1}$) is reported with a diode-laser-pumped, fiber-coupled, periodically poled LiNbO_3 spectroscopic source. This source replaced the Pb-salt diode laser Dewar assembly of an existing tunable diode-laser absorption spectrometer designed for ultrasensitive detection of CH_2O . Spectra are recorded with $2f$ -modulation spectroscopy and zero-air rapid background subtraction. Initial measurements reported here, determined from multiple measurements of a flowing 7.7 parts per billion by volume (ppbv, parts in 10^9) CH_2O in air mixture, indicate replicate precisions as low as 0.24 ppbv. © 2000 Optical Society of America
OCIS codes: 010.1120, 120.6200, 300.6340, 190.2620.

1. Introduction

Well-characterized tunable continuous-wave (cw) mid-IR laser sources are desirable for sensitive detection of trace atmospheric gases. Until recently, cryogenically operated Pb-salt diode lasers were the only mid-IR sources available in the 2–20- μm spectral region that fulfilled the strict criteria of narrow linewidth ($<100\ \text{MHz}$), low amplitude noise, an ability to be modulated at frequencies in the kilohertz-to-megahertz regime across spectral absorption features, and a power of more than several hundred microwatts. Using a Pb-salt diode laser gas sensor, Werle,¹ in the laboratory, measured absorption sensitivities of approximately 5×10^{-7} for NO_2 , employing high-frequency FM spectroscopy with an integration time of 25 s. This corresponds to a NO_2 detectable concentration limit of 0.010 parts per billion by volume (ppbv, parts in 10^9). Employing lower-frequency $2f$ spectroscopy, Fried *et al.*² reported routine field-monitoring sensitivities in the $1.5\text{--}2 \times 10^{-6}$ range for formaldehyde

(CH_2O), using an integration time of 20 s. This corresponds to a detectable concentration limit of 0.047–0.060 ppbv. Although these lasers lead to highly sensitive gas-detection devices, there are several important operational practicalities that need to be considered. For example, the Pb-salt diode structure is a Fabry-Perot cavity architecture, and as such there is no intrinsic wavelength stability to avert longitudinal mode hops. Furthermore, Pb-salt devices must be operated at low temperatures, typically between 77 and 150 K, and this requires a source of liquid nitrogen or continuous power in the case of new compact compressor cold heads. Since some cryogenically cooled Pb-salt lasers can exhibit dramatic changes in their output characteristics after temperature cycling, routine access to the spectral line of choice for monitoring a particular trace gas species requires holding the laser at one particular temperature for long periods of time. Attempts to maintain the Pb-salt lasers at cryogenic temperatures at all times to mitigate this tend to fail at some point over the laser lifetime. In addition, although one can readily obtain Pb-salt devices to hit numerous desired absorption features of interest, in some cases this comes at the expense of compromising one or more other desirable laser characteristics such as mode purity, laser power, mode stability, and moderate tuning rates, to name a few. The astigmatic, nonsymmetric nature of the emitted radiation from Pb-salt lasers can also lead to increased optical noise and interference effects. Moreover, the lasing area, $f/\#$, and lasing direction may vary from device to device, making it difficult to design an optimal optical system. Quantum cascade (QC) lasers,³ an emerging technology for direct generation of

When this research was performed, D. G. Lancaster and F. K. Tittel (fkt@rice.edu) were with the Electrical and Computer Engineering Department, Rice University, Houston, Texas 77005. A. Fried, B. Henry, and B. Wert were with the National Center for Atmospheric Research, Boulder, Colorado 80307. B. Wert was also with the Department of Chemistry, University of Colorado, Boulder, Colorado, 80309. D. G. Lancaster is now with the Defense Science and Technology Organization, P.O. Box 1500, Salisbury 5108, Australia.

Received 22 December 1999; revised manuscript received 26 May 2000.

0003-6935/00/244436-08\$15.00/0

© 2000 Optical Society of America

5–16- μm radiation, overcomes the longitudinal-mode stability issue by the inclusion of a distributed-feedback (DFB) grating. However, liquid-nitrogen cooling and the associated Dewar or cryogenic cold head are still required for narrow-bandwidth cw QC DFB laser operation. Although QC lasers should not be susceptible to temperature cycling, cryogenic operation adds considerable complexity to the optical system, as discussed below.

Difference-frequency generation (DFG) laser sources look particularly attractive as an alternative technique for generating coherent radiation at wavelengths in the 3–5- μm spectral region. These laser sources use readily available room-temperature near-IR single-frequency diode-laser-pump sources and a nonlinear optical material with a high figure of merit such as periodically poled LiNbO_3 (PPLN). Solid-state pump sources for DFG currently include diode-pumped Nd:YAG lasers, diode lasers or amplified diode-laser-pump sources,^{4–6} and rare-earth-doped fiber amplifiers.⁷ To improve ruggedness for field applications and to reduce the alignment and beam overlap requirements, it is desirable to use single-mode optical fibers and wavelength-division multiplexers for pump beam delivery and for convenient beam combining into a single fiber.⁸ Recent fiber-coupled DFG sources reported include an 11- μW DFG system in which the pump beams were amplified by an in-line diode-pumped Yb amplifier and a passive Er–Yb codoped fiber amplifier.⁹ A higher-power DFG system that generates as much as 0.7 mW by difference-frequency mixing of a Nd:YAG-laser-seeded Yb fiber amplifier and an Er–Yb fiber amplifier seeded by a 1560-nm DFB diode laser was recently reported.¹⁰

DFG laser sources have several advantages over Pb–salt diode lasers: These include removing the need for cryogenic cooling and the associated issues of temperature cycling, mode-hop-free operation, and the potential of significantly higher tunable mid-IR powers than the 100–200 μW of power typically available from Pb–salt lasers. Perhaps the most important single advantage of DFG laser sources over their Pb–salt counterparts is the potential for higher spatial beam quality, particularly the quality with which one collects, transforms, and ultimately couples the lasing beam through multipass absorption cells, which are often employed in field sensors for trace gas detection. In Pb–salt devices, as with QC lasers, the required cryogenic Dewar does not readily allow the primary collection optical element to be placed any closer than 14–19 mm from the laser-emitting surface without a significant amount of Dewar engineering. This distance constraint in turn necessitates a fairly big optical setup to collect and reduce the beam size and $f/\#$ to appropriate values for coupling into multipass absorption cells. In astigmatic Herriott cells, for example, which are becoming more popular in field diode laser spectrometers, the beam must pass through a small coupling hole, which typically ranges between 1 and 10 mm in diameter. Even in a relatively compact portable Pb–salt laser-based field instrument,¹¹ the requisite optical setup to achieve such coupling requires a 2

ft (0.61 m) \times 3 ft (0.91 m) optical bench. More compact systems can be devised, but this comes at the expense of an increased number of optical components that can independently become misaligned in a field system. By contrast, the optical collection element in DFG systems can be placed close enough to the PPLN crystal for direct coupling into a multipass cell without the need for additional beam-condensing optics. Moreover, the fiber-coupled PPLN input beams result in a nearly diffraction-limited Gaussian spot at the DFG focus. Not only do these attributes minimize the required optical setup and improve the beam coupling through multipass absorption cells; they also open up the possibility of integrally mounting the DFG laser source directly to the multipass absorption cell. The DFG beam-pointing stability should thus be dramatically improved, which will permit use of optical path-lengths that are longer than those currently employed for improved sensitivity.

Although the present CH_2O sensitivity (≈ 0.050 ppbv at the 1σ level for 20 s of averaging and ≈ 0.025 ppbv for 100 s) is quite good with a Pb–salt laser-based field instrument² employing optical pathlengths of 100 m, improving this sensitivity by at least a factor of 2 is important for more than academic reasons. Higher sensitivity, particularly on aircraft platforms, is needed to address discrepancies between published measurements and theoretical box-model calculations. Background measurements of CH_2O over remote ocean regions from various research groups employing different techniques are, with a few exceptions, consistently factors of 2–3 higher than concentrations predicted by theoretical box models (see Ref. 12 for a review of these comparisons). Since CH_2O is an important source of odd hydrogen radicals (OH and HO_2) to the atmosphere, such measurement-model discrepancies raise numerous questions regarding our knowledge of the chemistry involved as well as the veracity of the measurements themselves.

In addition to compactness, the potential for higher spatial beam quality and beam-pointing stability in a DFG-based sensor may make it possible to achieve the requisite sensitivities for ambient background measurements of CH_2O . However, to date, this aspect has not been thoroughly investigated. In fact, DFG laser sensors have not exploited many of the techniques recently employed with Pb–salt systems to improve measurement sensitivity such as wavelength modulation/second-harmonic detection, rapid background subtraction, and optical stabilization employing a temperature-stabilized enclosure. In the current study the performance of a DFG-based sensor using these techniques is scrutinized. To accomplish this, a DFG laser source was transported to the National Center for Atmospheric Research (NCAR) and replaced the Pb–salt diode laser Dewar assembly of an existing portable and robust sensor designed for ground-based and aircraft measurements of CH_2O . The original Pb–salt sensor is described in detail by Fried *et al.*,² and the modified system used here is described by Wert *et al.*¹¹ The performance of this sensor was extensively characterized in a ground-

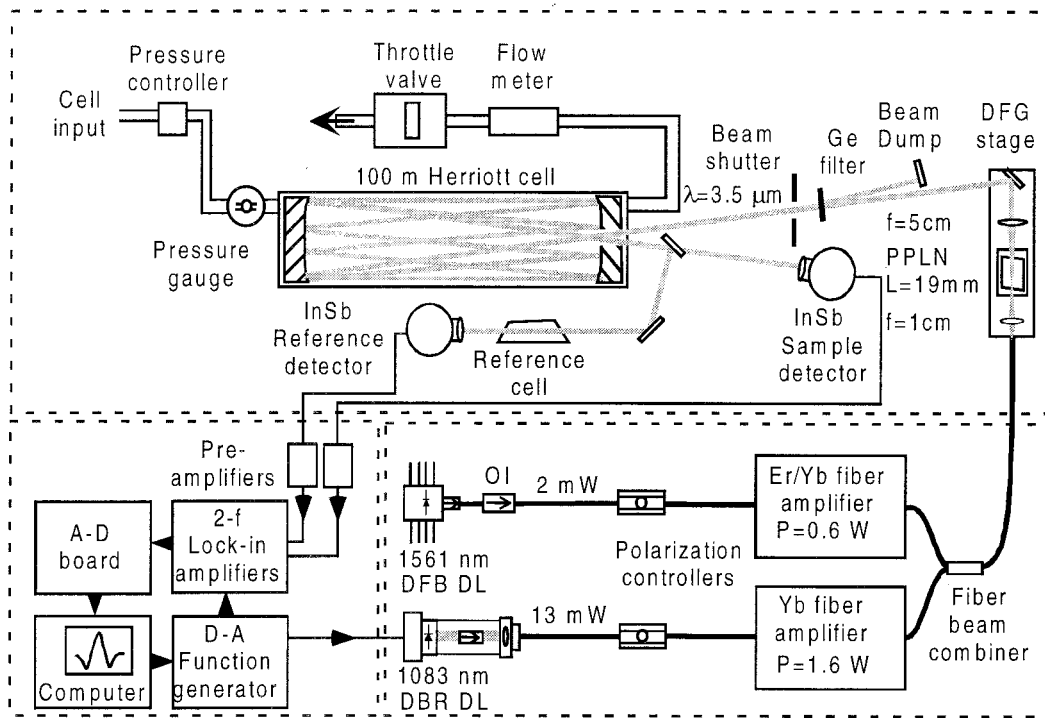


Fig. 1. Schematic of a DFG laser system incorporated in a dual-channel airborne tunable diode-laser absorption spectrometer, which normally employs a liquid-nitrogen-cooled Pb-salt diode laser. A-D, analog to digital; D-A, digital to analog; DL, diode laser; OI, optical isolator.

based study employing accurate low-level CH_2O standard mixtures in the ppbv range. The study described herein thus represents a good test case to allow for a direct intercomparison between a field-proven Pb-salt system with a DFG sensor by use of this same rigorous approach. Although the DFG sensor discussed here exhibited some operational problems and although the potential improvements in beam quality and pointing stability, discussed above, could not be implemented here, the current study provides a much needed starting point for accurately assessing the performance of a DFG-based gas sensor.

2. Description of the Difference-Frequency Generation Laser Source Coupled to the Existing Field-Detection System

A schematic of the DFG-based, $2f$ -wavelength-modulation spectroscopic configuration is shown in Fig. 1. The overall sensor consisted of a small optical table [18 in. (46 cm) \times 12 in. (30 cm)] containing the DFG pump sources and driver electronics, as well as the fiber optics for beam combining and polarization control. A larger temperature-controlled enclosure contained the difference-frequency stage, beam delivery and collection optics, multipass cell, and detectors. This enclosure surrounded the entire optical assembly, including the optical bench. The data-acquisition and processing electronics, including the lock-in amplifiers, digital-to-analog converter for waveform generation, analog-to-digital converters for signal digitization, and data-acquisition computer, were mounted below the optical enclosure.

The mid-IR DFG source was based on low-power

diode-laser sources at 1 and 1.5 μm , which seeded 1.5-W Yb and 0.6-W Er-Yb fiber amplifiers, respectively. One seed source was a 50-mW 1083-nm distributed Bragg reflector diode laser, and 13 mW of its output was coupled into a single-mode fiber to seed the 1.6-W Yb amplifier after passing through two bulk optoisolators with a combined isolation of -70 dB. A 2-mW fiber-pigtailed 1561-nm DFB telecommunications diode laser with -80 dB of isolation provided by two pigtailed optical isolators was used to seed the 0.6-W Er-Yb fiber amplifier. To minimize backreflections into the high-gain amplifiers and prevent formation of optical etalons, all optical fiber terminations used in the sensor were terminated with connectors that have their ends polished at 8° off normal incidence. In-line polarization controllers were placed on each input fiber to set the linear vertical polarization states required for quasi phase matching. Polarization was maintained during DFG operation, provided that the fibers were not subject to mechanical or acoustic vibrations. The output from each fiber amplifier was combined into a single fiber by use of a fiber wavelength-division multiplexer. The rare-earth amplifiers are based on Yb and Er-Yb-doped double-clad fibers pumped by 4-W 975-nm diode lasers and described in Ref. 7.

The optical components and PPLN crystal required for DFG generation were mounted on an 8 in. (20 cm) \times 2.5 in. (6.35 cm) aluminum base plate, which in turn was mounted in the temperature-controlled enclosure in place of a Pb-salt diode-laser Dewar assembly. The modified optical setup is shown in Fig. 1. A single optical fiber delivered the combined

pump beams. The fiber output was imaged by an $f = 10$ -mm antireflection- (AR-) coated achromat lens (magnification, 11) into a 19-mm-long PPLN crystal. The PPLN crystal, which contained nine quasi-phase-matched channels with periods ranging from 29.7 to 30.5 μm in 0.1- μm increments, was mounted on a Peltier element for temperature control and AR coated for pump, signal, and idler wavelengths. Phase-matching conditions for generation of 2831.64- cm^{-1} (3.532- μm) radiation occurs at a domain period of 30.1 μm and $T = 34$ °C. The generated light was collimated by an $f = 5$ cm CaF_2 lens, and the residual pump light was removed by an AR-coated Ge filter.

The mid-IR light was then directed through a 100-m-path-length astigmatic Herriott cell (throughput efficiency, $\approx 8\%$) and was incident on a cryogenically cooled InSb detector. A beam splitter directed $\approx 10\%$ of the light to a second InSb detector through a 5-cm-long reference cell containing a small amount of *para*- CH_2O in ≈ 20 Torr of air (wavelength reference).

The laser control and the data handling were integrated into one computer-controlled system. The DFG wavelength was scanned with a 200-point sawtooth waveform (≈ 0.15 cm^{-1}) across an isolated CH_2O absorption line (to be discussed) at 50 Hz. A 50-kHz quasi-square-wave-modulation waveform was simultaneously applied to the laser tuning current. Scanning and modulation waveforms were provided by a 12-bit digital-to-analog board, which directly modulated one of the pump diode current controllers. The signals at twice the modulation frequency ($2f = 100$ kHz) were recorded with two ac-coupled commercial lock-in amplifiers employing a time constant of 0.3 ms. The amplifier outputs were then digitized by a 16-bit analog-to-digital card sampling at 10 kHz and interfaced to a Pentium II computer running LabVIEW software code (National Instruments) and MS Windows98. To normalize laser power variations, the sample detector dc photocurrent was measured on every scan, and every few minutes the beam shutter following the Ge filter of Fig. 1 was closed to capture the sample detector dark current. The laser power in the sample arm was determined from the difference between the two photocurrents. In all cases the dark current was less than 8% of the detector signal in the presence of laser light.

The Herriott cell continuously sampled at flow rates near 8.8 standard liters min^{-1} (slm, where standard conditions are defined as $T = 273$ K and $P = 760$ Torr). An inlet pressure controller maintained the cell pressure at 40 Torr, and cell temperatures near 23 °C were employed. The cell temperature, as measured with a calibrated platinum resistance temperature detector (RTD) probe mounted on the cell wall, was not actively controlled for these measurements. However, because the entire optical setup was mounted in a temperature-insulated box, the active temperature throughout these measurements was constant. In addition to the cell temperature, the enclosure and/or optical bench temperatures were measured at seven different locations with calibrated RTD probes. Throughout any given mea-

surement run, the maximum standard deviation in any of these probes was always less than 0.3 °C, and more typically less than 0.1 °C.

CH_2O -free zero air was generated by means of passing ambient laboratory air through a heated $\text{Pd-Al}_2\text{O}_3$ catalytic converter, as further described in Refs. 13–15. This unit effectively removes CH_2O without appreciably affecting the ambient water-vapor concentration. The zero air was added to the inlet line a few inches from the inlet tip at flow rates ~ 3 slm higher than the cell flow. Calibrated CH_2O mixtures were generated in the inlet by means of injecting the output flow of a CH_2O permeation system into the inlet downstream of the zero-air addition point. In this procedure calibration flow of ~ 0.4 slm continuously passed through a 0.125-in. (~ 0.317 -cm) Teflon union T , close to the standards addition point. When required, we sampled zero air without addition of CH_2O by drawing off the calibration flow. For this purpose the calibration flow plus an additional ~ 0.6 slm of zero air was drawn out the side of the union T and through a 1-slm flow controller with a pump. References 13–15 give further details of this procedure.

After dilution with zero air in the inlet, CH_2O standards at two different concentrations (14.3 and 7.7 ppbv) were generated in this study with employment of two different permeation devices. The higher concentration standard served as the calibration source to which the lower-level standard was fit. As further discussed below, the lower-level standard was repetitively sampled and treated analogously to an ambient sample. Such measurements are hereafter designated pseudoambient samples. Numerous tests have been carried out in both the laboratory and the field to ensure uniform mixing of the standard in the inlet line. Furthermore, as discussed in Fried *et al.*² and references therein, the CH_2O permeation standards were verified with four independent techniques and have an estimated total uncertainty of 6% (at the 1 σ level). Generation of low-level standards and knowledge of the absolute concentration are essential for accurately assessing the performance of the DFG sensor employed in this study.

3. Difference-Frequency Generation Absorption Spectrometer: Performance Evaluation

As much as 220 μW of cw radiation was generated at 3.5 μm (2832 cm^{-1}) for incident pump powers of 800 and 260 mW at 1 and 1.5 μm , respectively, at the PPLN crystal.¹⁰ However, only 25–30 μW was available for these experiments at NCAR, owing to a problem with the 1.5- μm fiber amplifier (a misalignment of the pump-laser-coupling lens in the sealed fiber amplifier package that occurred during shipping of the sensor from Houston to Boulder). Unfortunately, the repair, which was impossible to effect in the field, could not be accomplished in time for the current measurements.

For these comparative measurements the DFG source was tuned to an isolated CH_2O line at 2831.64 cm^{-1} (3.5315 μm) with an integrated absorption cross section of 5.59×10^{-20} cm^2 cm^{-1} molecule⁻¹ ($T = 296$

K, and application of Sams +11% correction factor is as given in Ref. 16). As discussed by Fried *et al.*² and references therein, the CH₂O line at 2831.64 cm⁻¹ is clear of any known spectral interference with the exception of a small potential bias from H₂O (to be discussed). However, since then, the Rice University–NCAR team has discovered the presence of a weak methanol feature (CH₃OH) that is not listed in the 1996 HITRAN database¹⁷ and that is adjacent to the CH₂O line. Subsequent laboratory measurements carried out at NCAR indicate that the CH₃OH feature produces a 3.9% positive error in the retrieved CH₂O concentrations. Ambient CH₃OH concentrations in the remote background atmosphere typically fall within the range of 50–800 parts in 10¹² by volume (Jaeglé *et al.*),¹⁸ and thus the CH₃OH interference should produce a maximum error of 0.031 ppbv on ambient CH₂O measurements. However, typical errors due to the CH₃OH interference in the background atmosphere should be of the order of 0.015 ppbv.

The potential small H₂O interference mentioned above results from a line 0.1993 cm⁻¹ higher in frequency and a factor of 5.2×10^{-5} weaker in strength than the above CH₂O feature. Employing sampling pressures near 25 Torr and second-harmonic detection, Fried *et al.*² determined that H₂O concentrations as high as 2% do not cause interference during quantification of ambient CH₂O concentrations as low as 0.1 ppbv. Employing sampling pressures near 40 Torr, which we now use for increased sensitivity, results in a +6% error in the retrieved second-harmonic CH₂O levels.² This error, however, is completely eliminated when we employ our rapid background-subtraction approach, using the catalytic converter mentioned above. Because the ambient H₂O concentration is relatively constant in both ambient and background acquisition modes, the small H₂O contribution to the second-harmonic signal is effectively removed. Other features listed in the 1996 HITRAN database, as well as numerous other organic molecules tested at NCAR (ethanol, 2-propanol, acetaldehyde, propanal, butanal, acetone, and methyl ethyl ketone) do not exhibit any spectral interference during measurement of CH₂O employing the 2831.6417-cm⁻¹ line with the sampling conditions detailed above. Although other wavelength regions may also be useful for ambient measurements of CH₂O, at present we have not been able to identify a better candidate line that is simultaneously strong and devoid of spectral interferences. Absorption features in the 1760-cm⁻¹ region may satisfy these requirements; however, at present only preliminary line assignments and strengths are available.

Rapid background subtraction was used to acquire the results of the current study. As discussed by Fried *et al.*,² this approach has been shown to be effective in capturing and removing time-varying optical noise in a Pb–salt diode-laser system. Such noise, which ultimately limits the performance of most if not all highly sensitive absorption spectrometers, is caused by light scattering from various optical elements. In some cases scattering from a single element dominates, and this produces a classic etalon

fringe. In most instances, such optical noise contains multiple frequencies, amplitudes, and time constants, originating from multiple scattering sources, and this generates more subtle time-varying background structure. The optical noise encountered in the current study exhibits both types of behavior. The optical noise sources are discussed in Section 4.

In our typical data-acquisition approach a 14.3-ppb-calibration spectrum was first acquired with a 20-s integration period. Background spectra (10-s integrations) before and after the calibration were acquired by use of the zero-air catalytic converter discussed above. The backgrounds were averaged and subtracted point by point from the calibration spectrum. Next, sample mixtures, with either the 7.7-ppbv pseudoambient standards or zero air, were repetitively sampled. Each determination was made up of a 20-s sample measurement along with two 10-s background acquisitions before and after each sample. A 6-s flushing period, to allow for complete sample exchange in the cell (≈ 5 -folding time periods), was implemented before and after each background. Including computer overhead time, each sample acquisition thus acquired spanned approximately 1 min. We hereafter refer to each such sample acquisition as a 1-min determination.

As with the calibration, the backgrounds surrounding each sample were averaged and subtracted point by point from the sample spectrum. As shown in Fig. 3 of Fried *et al.*,² the average background surrounding each sample in most cases more effectively

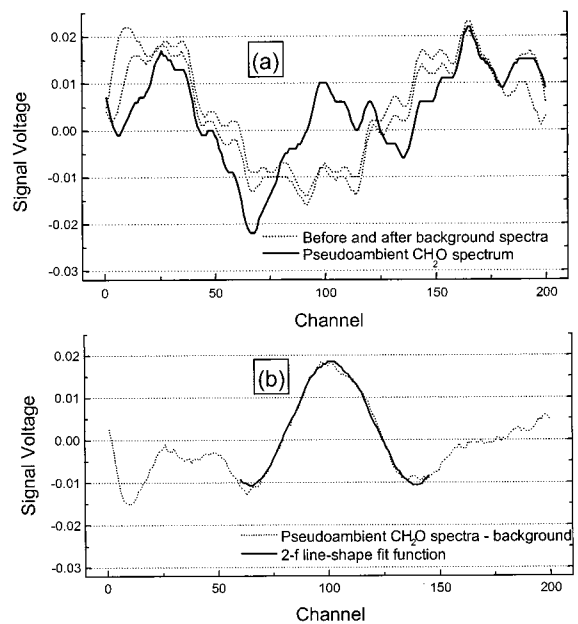


Fig. 2. (a) 20-s spectrum (solid curve), obtained by sampling of a 7.73-ppbv CH₂O standard, and backgrounds (dotted curves) taken before and after (10-s averages). (b) Resultant CH₂O spectrum with the averaged-background spectrum subtracted (dotted curve) and the fit second-harmonic profile (solid curve). The spectra are plotted in terms of channel number. For reference the 2831.642-cm⁻¹ line center appears near channel 100, and the resolution of the display is approximately 7×10^{-4} cm⁻¹ channel⁻¹.

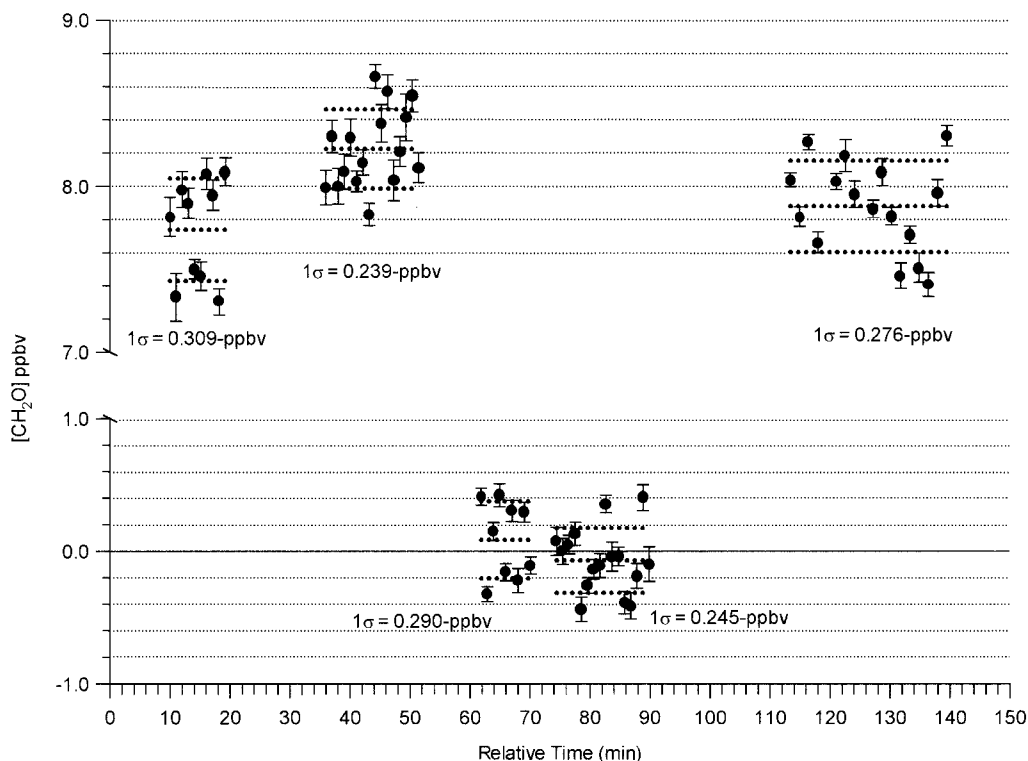


Fig. 3. DFG sensor-based replication precision for CH_2O standards of ~ 7.7 and 0 ppbv employing second-harmonic detection along with rapid background subtraction. The mean fit values along with the upper and the lower 1σ precision for each measurement block are given by the dotted lines. The block replication precisions are also indicated below each block. The individual data points for the first four blocks are made up of two 10-s background spectra and one 20-s sample spectrum (see text). In the final measurement sequence on the right-hand side the sample and background averaging times were increased to 30 and 20 s, respectively. Error bars denote the 1σ fit precisions for each measurement.

captures the true background underlying the sample spectrum than a single background. After the background-subtracted sample spectra were corrected for laser power drifts, each sample spectrum was fit (in time space) to the background-subtracted calibration spectrum previously acquired. Fitting was achieved by employment of a multiple linear regression approach with singular-value decomposition, as described by Sewell *et al.*¹⁹ In this procedure each sample spectrum second-harmonic line profile was fit to that obtained for the high-concentration calibration spectrum. An appropriate scale coefficient was obtained from the best-fit regression parameters, which when multiplied by the calibration concentration yielded a fit concentration. This procedure was carried out in real time.

Typical second-harmonic CH_2O spectra (Fig. 2, solid curve) acquired for a single 20-s pseudoambient measurement ($\text{CH}_2\text{O} = 7.73$ ppbv) along with surrounding 10-s background spectra are shown in Fig. 2(a). The spectra are plotted in terms of channel number. For reference the 2831.642-cm^{-1} line center appears near channel 100, and the resolution of the display is approximately $7 \times 10^{-4} \text{ cm}^{-1} \text{ channel}^{-1}$. The dotted curves represent the backgrounds before and after the sample measurement. Because the background traces are nearly identical in shape, they accurately capture the background underlying the sample spectrum. Figure 2(b) displays the

pseudoambient CH_2O trace [solid curve in Fig. 2(a)] minus the average of the two background spectra [dotted curves in Fig. 2(a)] along with the results of fitting the 7.73-ppbv pseudoambient sample to the 14.3-ppbv calibration standard (solid curve).

Measurement performance was obtained by calculation of the replication precision (σ_r , at the 1σ level) for blocks of measurements for which the input concentration was held constant. The fit precision, σ_f , which is related to the squared-fit deviations, was also determined from the singular-value-decomposition-retrieval. Figure 3 displays the results for five different measurement blocks acquired at two different input CH_2O concentrations. Each measurement block is made up of 9–16 individual 1-min determinations. The mean fit value along with the upper and the lower $1\sigma_r$ bounds are displayed for each measurement block by the dotted lines, and the σ_r values are also given beneath each measurement block. The fit precisions, which are also displayed, are denoted by the error bars on each individual 1-min determination. As can be seen, the replication precision at both CH_2O levels yields consistent results within the 0.239–0.309-ppbv range. By contrast, the fit precision, which is sometimes employed by investigators as a measure of performance, yields overly optimistic results by a factor of 3–4. As discussed by Fried *et al.*,² the fit precision and/or the high-frequency noise in the

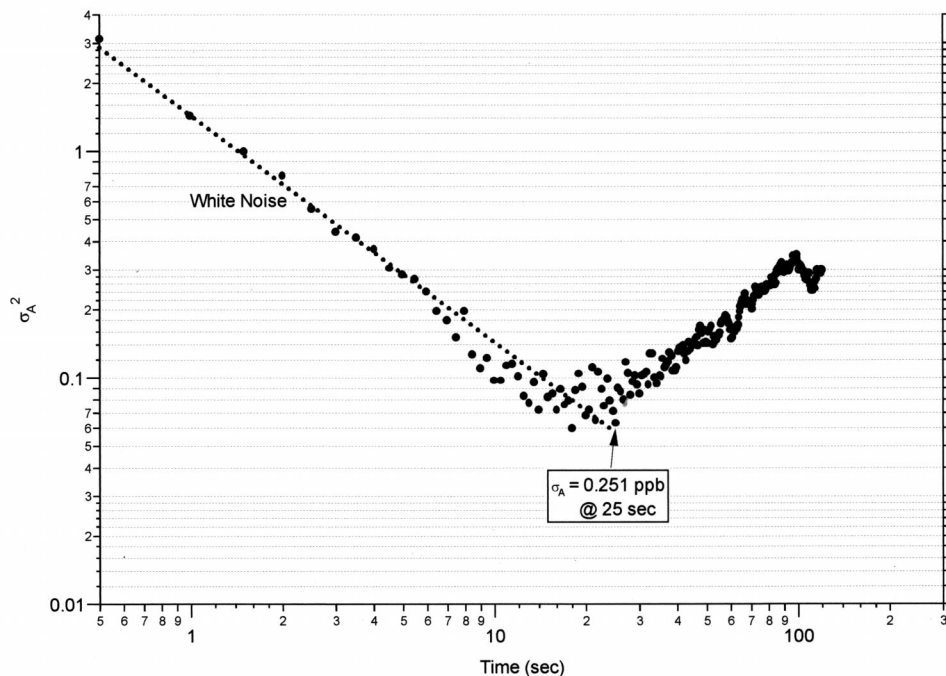


Fig. 4. Allan variance plot generated by acquisition and subsequent fitting of 0.5-s sample averages for a 7.7-ppbv CH_2O standard. The measurements show a system stability period of 25 s before systematic drifts become evident. At shorter time periods the Allan variance, σ_A , improves by time^{-1} , as expected from white noise. The square root of the Allan variance indicates a system detection limit of 0.251 ppbv for an integration time of 25 s.

wings of an absorption feature does not adequately capture run-to-run imprecision.

An Allan variance plot, generated by repetitive acquisition of 0.5-s samples for the 7.7-ppbv CH_2O standard, is shown in Fig. 4. This plot, which is nearly identical to a second plot run immediately after Fig. 4, shows a linearly decreasing Allan variance (σ_A^2) out to ~ 25 s, which represents the white-noise-dominated regime. This result indicates that the sensor is stable for ~ 25 s, hence indicating the total acquisition sequence time for optimum sensitivity. At this integration time the square root of the Allan variance indicates a detection limit of 0.251 ppbv, similar to the results of Fig. 3. However, four of the five block averages of Fig. 3 were obtained with effective integration times (time between the start of the first background to the end of the second background acquisition) of ~ 60 s. The effective integration time for the fifth block average (the measurement block on the right-hand side of Fig. 3) was ~ 90 s. An additional measurement carried out on a previous day with an even shorter effective integration time of ~ 32 s resulted in a replication precision of 0.371 ppbv. Apparently there is some variability in the stability period for the present DFG sensor that needs to be explored further. Nevertheless, the measurement precisions as well as the Allan variance results all point to a 1σ CH_2O precision in the 0.2–0.4-ppbv range.

4. Discussion

The cw tunable DFG-based absorption spectrometer at this time is less sensitive by a factor of approximately

4–5 than typical results obtained with a cryogenically cooled Pb–salt diode laser when used in the same configuration at NCAR with the same data-acquisition strategy. However, a number of obvious problems in the DFG mid-IR spectroscopic source can be identified. These include reduced mid-IR power available during these experiments and low-frequency optical noise, which tended to distort the symmetry of the $2f$ line shape. A source of optical noise from scattering are the three refractive optical elements in the DFG stage (the input and output coupling lenses and the PPLN crystal). The individual spectral fits showed clear signs of such noise, which was manifested by a randomly undulating background structure that changed erratically with each series of measurements. Fortunately, the two PPLN coupling lenses can be replaced with off-axis reflective elements, which should eliminate the optical noise contribution from this source. Furthermore an improved AR coating on the PPLN crystal will reduce the high level of scattering, which is observed from the current coatings on the crystal.

An alternative approach to reduce the magnitude of the optical noise attributed to scattering from the optical surfaces is to run each amplifier in a highly saturated mode with optically isolated preamplifiers to boost the seed powers from the 1083- and 1561-nm diode lasers. Hence the amplifiers would become significantly less susceptible to feedback from these surfaces. Finally, a low sensor power of 25 μW resulted in only ~ 2 μW of power incident on the detector. Consequently, our preliminary measurements were limited in part by detector thermal noise. With more power available, longer absorption pathlengths will be

viable, and the signal to noise from the detectors will be substantially increased.

5. Conclusions

In summary, we have demonstrated that a DFG-based mid-IR spectrometer using second-harmonic detection and rapid background subtraction reproducibly achieves a 1σ measurement precision in the 0.2–0.4-ppbv range for detection of formaldehyde (CH_2O). Most of the measurements fell within the 0.2–0.3-ppbv range. At the sampling conditions of pressure (40 Torr), temperature (296 K), and pathlength (100 m) this corresponds to a minimum detectable absorbance (1σ level) in the $0.7\text{--}1.3 \times 10^{-5}$ range. This is comparable with precisions of ~ 0.050 -ppbv when a liquid-nitrogen-cooled Pb-salt diode laser is employed with the same data-acquisition and data-reduction approaches. However, a number of improvements have been identified to the current *ad hoc* DFG setup, and it is expected that an optimized cw DFG laser system should, at the very least, approach, if not surpass, the level of performance routinely obtained with the Pb-salt diode laser system. In fact, recent measurements by one of the current authors (D. G. Lancaster) indeed suggest that further improvements are realistic. Although these improvements could not be implemented in time for the current measurements, the results presented here are useful for providing a good starting point for the realistic assessment of DFG performance and for providing the first direct comparison of the two laser technologies.

The National Center for Atmospheric Research (NCAR) is sponsored by the National Science Foundation. In addition, the development of the mid-IR source performed at Rice University was supported by NASA, the Texas Advanced Technology Program, the Welch Foundation, Gulf Coast Hazardous Substance Research Center, and the National Science Foundation. The authors thank Lew Goldberg with the Naval Research Laboratory for providing us with the fiber amplifiers and Paul Williams of the National Institute of Standards and Technology (NIST) for the timely loan of a fiber splicer.

References

1. P. Werle, R. Mucke, and F. Slemr, "The limits of signal averaging in atmospheric trace-gas monitoring by tunable diode-laser absorption spectroscopy," *Appl. Phys. B* **57**, 131–139 (1993).
2. A. Fried, B. Henry, B. Wert, S. Sewell, and J. R. Drummond, "Laboratory, ground-based, and airborne tunable diode laser systems: performance characteristics and applications in atmospheric studies," *Appl. Phys. B* **67**, 317–330 (1998).
3. F. Capasso, C. Gmachl, D. L. Sivco, and A. Y. Cho, "Quantum cascade lasers," *Phys. World* **12**, 27–33 (1999).
4. K. P. Petrov, L. Goldberg, W. K. Burns, R. F. Curl, and F. K. Tittel, "Detection of CO in air by diode-pumped 4.6- μm difference-frequency generation in quasi-phase-matched LiNbO_3 ," *Opt. Lett.* **21**, 86–88 (1996).
5. D. Richter, D. G. Lancaster, R. F. Curl, W. Neu, and F. K. Tittel, "Compact mid-infrared trace gas sensor based on difference-frequency generation of two diode lasers in periodically poled LiNbO_3 ," *Appl. Phys. B* **67**, 347–350 (1998).
6. U. Simon, F. K. Tittel, and L. Goldberg, "Difference-frequency mixing in AgGaS_2 by use of a high-power GaAlAs tapered semiconductor amplifier at 860 nm," *Opt. Lett.* **18**, 1931–1933 (1993).
7. L. Goldberg, J. Koplow, and D. A. V. Kliner, "Highly efficient 4-W Yb-doped fiber amplifier pumped by a broad-stripe laser diode," *Opt. Lett.* **24**, 673–675 (1999).
8. D. G. Lancaster, L. Goldberg, J. Koplow, R. F. Curl, and F. K. Tittel, "Fibre coupled difference frequency generation utilizing a ytterbium-doped fibre amplifier and periodically poled LiNbO_3 ," *Electron. Lett.* **34**, 1345–1346 (1998).
9. L. Goldberg, J. Koplow, D. G. Lancaster, R. F. Curl, and F. K. Tittel, "Mid-infrared difference-frequency generation source pumped by a 1.1–1.5- μm dual-wavelength fiber amplifier for trace-gas detection," *Opt. Lett.* **23**, 1517–1519 (1998).
10. D. G. Lancaster, D. Richter, R. F. Curl, F. K. Tittel, L. Goldberg, and J. Koplow, "High-power continuous-wave mid-infrared radiation generated by difference frequency mixing of diode-laser-seeded fiber amplifiers and its application to dual-beam spectroscopy," *Opt. Lett.* **24**, 1744–1746 (1999).
11. B. Wert, A. Fried, B. Henry, and J. R. Drummond, "Enhancement of a tunable diode laser tropospheric trace gas measurement system," in *Application of Tunable Diode and Other Infrared Sources for Atmospheric Studies and Industrial Processing Monitoring*, A. Fried, ed., Proc. SPIE **3758**, 100–108 (1999).
12. A. Fried (National Center for Atmospheric Research, Boulder, Colo. 80307), Y.-N. Lee, G. Frost, B. Wert, B. Henry, J. R. Drummond, M. Trainer, and F. Fehsenfeld are preparing a manuscript to be called "Airborne CH_2O measurements over the North Atlantic during the 1997 NARE campaign: instrument comparisons and distributions."
13. A. Fried, B. Wert, B. Henry, and J. R. Drummond, "Airborne tunable diode laser measurements of trace atmospheric gases," in *Fabrication, Testing, and Reliability of Semiconductor Lasers III*, Proc. SPIE **3285**, 154–162 (1998).
14. A. Fried, B. Henry, J. R. Drummond, G. Frost, and Y.-N. Lee, "Airborne tunable diode laser measurements of formaldehyde during the 1997 North Atlantic Regional Experiment," in *Application of Tunable Diode and Other Infrared Sources for Atmospheric Studies and Industrial Processing Monitoring II*, A. Fried, ed., Proc. SPIE **3758**, 90–99 (1999).
15. A. Fried, B. Wert, B. Henry, and J. R. Drummond, "Airborne tunable diode laser measurements of formaldehyde," *Spectrochim. Acta Part A* **55**, 2097–2110 (1999).
16. R. Sams, "Line strengths of some selected transitions in the 2900 cm^{-1} region of H_2CO ," in *Tunable Diode Laser Spectroscopy, Lidar, and DIAL Techniques for Environmental and Industrial Measurements*, A. Fried, D. K. Killinger, and H. I. Schiff, eds. Proc. SPIE **2112**, 62–69 (1993).
17. L. S. Rothman, C. P. Rinsland, A. Goldman, S. T. Massie, D. P. Edwards, J. M. Flaud, A. Perrin, C. Camy-Peyret, V. Dana, J.-Y. Mandin, J. Schroeder, A. McCann, R. R. Gamache, R. B. Wattson, K. Yoshino, K. V. Chance, K. W. Jucks, L. R. Brown, V. Nemtchinov, and P. Varanasi, "The HITRAN molecular spectroscopic database and HAWKS (HITRAN atmospheric workstation): 1996 edition," *J. Quant. Spectrosc. Radiat. Transfer* **60**, 665–710 (1998).
18. L. Jaeglé, D. J. Jacob, W. H. Brune, I. Faloon, D. Tan, B. G. Heikes, Y. Kondo, G. W. Sachse, B. Anderson, G. L. Gregory, H. B. Singh, R. Pueschel, G. Ferry, D. R. Blake, and R. Shetter, "Photochemistry of HO_x in the upper troposphere at northern midlatitudes," *J. Geophys. Res.* **105**, 3877–3892 (2000).
19. S. Sewell, A. Fried, B. Henry, and D. R. Drummond, "A field diode-laser spectrometer employing an astigmatic Herriot cell," in *Tunable Diode Laser Spectroscopy, Lidar, and DIAL Techniques for Environmental and Industrial Measurements*, A. Fried, D. K. Killinger, and H. I. Schiff, eds., Proc. SPIE **2112**, 72–80 (1993).